

Energy-efficient synthesis of $Ti_3C_2T_x$ MXene for electromagnetic shielding

H. Renuka ^a, Morgan Chen ^a, Shwetha Sunil Kumar ^a, Long Yang ^b, Michael T. Lanagan ^c, Sanjit Ghose ^d, B. Reeja-Jayan ^{a,*}

^a Department of Mechanical Engineering, Carnegie Mellon University, Pittsburgh, PA, 15213, USA

^b School of Materials Science and Engineering, Tongji University, Shanghai, 201804, China

^c Materials Research Institute, The Pennsylvania State University, University Park, PA, 16802, USA

^d Brookhaven National Laboratory, National Synchrotron Light Source II, Upton, NY, 11973, USA

ARTICLE INFO

Keywords:
2D materials
Green synthesis
Microwave chemistry
EMI shielding
Pair distribution function

ABSTRACT

Traditional methods for synthesizing two-dimensional $Ti_3C_2T_x$ MXenes such as hydrofluoric acid (HF) or LiF/HCl based etching can be time-consuming, complex, and often result in low yields. They generally involve multi-step processes involving >40 h of preparation time that can expose the materials to harsh conditions. In this study, we demonstrate a rapid single-step microwave (MW) synthesis method that significantly reduces production time to 90 min, achieving a 90 % yield and cutting energy consumption by 75 %. For the first time, synchrotron x-ray pair distribution function (PDF) analysis conducted on MW-synthesized MXene (MW- $Ti_3C_2T_x$) indicates greater structural fidelity in local atomic ordering, indicating high-quality which is comparable to conventionally synthesized counterparts (CO- $Ti_3C_2T_x$). This method achieves similar or greater structural quality in less time while also enhancing electromagnetic interference shielding (EMI SE) performance. A 15 μm MW- $Ti_3C_2T_x$ film demonstrated an impressive EMI SE of ~67 dB in the X-band, compared to the ~63 dB achieved by CO- $Ti_3C_2T_x$. The enhanced EMI SE performance is attributed to the presence of fluorine terminations, which provide oxidation resistance, increased conductivity and improved absorption of EM waves. The MW-induced shocks during irradiation not only help remove O_2/OH groups, preventing oxidation, but also tunes the functional groups, enhancing charge transport and effective EM wave attenuation. The MW synthesis method presents a fast, efficient, and scalable approach for producing high-quality MXene nanosheets, paving the way for advancements in EMI shielding and other applications.

1. Introduction

Two dimensional (2D) materials such as graphene, transition metal dichalcogenides (TMD's) and hexagonal Boron Nitride (hBN) have garnered renewed research interest in the past decade [1–3]. Recently, MXenes have captivated the scientific community owing to their exceptional chemical, electrical, optical and mechanical properties and their applications in various fields, such as sensing, electrochemical energy storage, water splitting, memory devices, and many more [4–6]. MXenes, a family of 2D transition metal carbides or nitrides, are represented by the general formula $M_{n+1}X_nT_x$, where M refers to an early transition metal, X carbon and/or nitrogen and T represents surface termination groups with $n = 1, 2$ or 3 and $x =$ number of terminal groups [7]. Among various MXene materials, $Ti_3C_2T_x$ stands out as a prominent electromagnetic interference (EMI) shielding material due to its excellent electrical conductivity, high dielectric constant and tunable surface

chemistry [8,9]. Additionally, the ability to create lightweight flexible freestanding films enhances its potential as a superior EM shield [10]. Many articles have investigated the EM shielding effectiveness (SE) of $Ti_3C_2T_x$ [11–13]. For example, Shazad et al. reported a high 92 dB in 45 μm thick $Ti_3C_2T_x$ MXene films and importantly 9 μm $Ti_3C_2T_x/SA$ nanocomposite film with a $Ti_3C_2T_x$ mass fraction of 90 wt% exhibited 57 dB of EMI SE [14]. Similarly, Zhang et al. demonstrated that a blade coated 940 nm thick film can achieve ~50 dB EM performance [15]. Furthermore, MXene/SA foam structures coated with PDMS exhibited shielding efficacy reaching 70.5 dB [16]. While existing research highlights the potential of MXenes and their composites as effective EM radiation shields, there is a significant gap in understanding the efficiency of MXene production processes.

To date, the predominant method for synthesizing $Ti_3C_2T_x$ is a lengthy two-step process; selective etching followed by delamination of the MAX phase [8,17]. The etching process is quite slow, often taking

* Corresponding author.

E-mail address: bjayan@andrew.cmu.edu (B. Reeja-Jayan).

more than 48 h to complete [18]. Furthermore, delamination influences the lateral size of MXene flakes, with larger dimensions requiring an extended process. Moreover, the use of organic intercalants demands additional washing time to achieve pristine $\text{Ti}_3\text{C}_2\text{Tx}$ flakes [19–21]. A recent cradle-to-gate life cycle assessment performed on $\text{Ti}_3\text{C}_2\text{Tx}$ showed that electricity consumption is the primary factor contributing to the environmental footprint [22]. The study estimated that for large-scale batches, electricity accounted for more than 70 % of the environmental impact, and for small batches, it exceeded 90 % [22]. This significantly restricts the utility of MXene-based applications in practical environments, especially where long-term operation is required. Therefore to mitigate these concerns, reducing energy consumption and accelerating synthesis are necessary. Moreover, the synthesis method significantly influences MXene properties, including surface termination, composition, flake size, conductivity, and degradation resistance [23]. Therefore, developing a rapid, energy-efficient process to produce high-quality $\text{Ti}_3\text{C}_2\text{Tx}$ is crucial to address these challenges.

Recently, microwave chemistry has emerged as a rapid and efficient technique for producing functional nanomaterials [24]. For example, Cai et al. showed that microwave (MW) irradiation effectively reduces graphene oxide (GO) to reduced graphene oxide (rGO) within a MXene matrix [25]. Similar investigations by Zhu et al. and Numan et al. have presented MW-assisted synthesis as a promising approach for MXenes [26,27]. While these investigations demonstrated the potential of this technique, it is not clear how MWs interact with the MAX phase during etching or how the surface terminations are affected thereby leading to uncertainties about the reproducibility of the process under different conditions. There are still critical gaps remaining, including the long-term stability and durability of MW-synthesized MXenes for high demand applications such as EMI shielding. Therefore, the objectives of this study are to establish a fast, scalable and energy efficient synthesis process for $\text{Ti}_3\text{C}_2\text{Tx}$ MXenes, focusing on improving the quality, and functional properties. This study also aims to assess the long-term stability and durability of the synthesized MW-MXenes while exploring the underlying mechanisms.

In this work, we present a rapid single-step MW-method for synthesizing exfoliated $\text{Ti}_3\text{C}_2\text{Tx}$ nanosheets (NS) in under 90 min. The MW- $\text{Ti}_3\text{C}_2\text{Tx}$ films have been further tested for EMI SE performance at various film thickness. The MW-approach not only accelerates the etching of MAX (Ti_3AlC_2) phase but also reduces energy consumption by ~75 % and achieves a remarkable 90 % yield (see supplementary information for energy and cost analysis). Furthermore, this process effectively removes O₂/OH terminal groups from Ti-sites within the MXene structure, thereby reducing the availability of oxidation sites. The elevated pressure inside the MW reactor vessel aids in the further exfoliation of MXene sheets, enhancing the fluorine termination on the MXene surface and increase in inter-sheet spacing [27].

X-ray diffraction (XRD) analysis confirms complete elimination of aluminium (Al) compared to MXenes synthesized from conventional process (CO- $\text{Ti}_3\text{C}_2\text{Tx}$) which showed residual Al even after extended hours of etching (~18 h). High-energy synchrotron X-ray pair distribution function (PDF) analysis was carried out for the first time on MW-synthesized MXenes to supplement XRD by further probing the short-range atomic ordering of the MXene samples. The results indicate that the local atomic arrangements of the MW- $\text{Ti}_3\text{C}_2\text{Tx}$ resemble the ideal Ti_3C_2 structure more so than that of the conventional (CO-MXene) ones, validating that MW- $\text{Ti}_3\text{C}_2\text{Tx}$ are of higher structural quality. Both the MW- and CO- $\text{Ti}_3\text{C}_2\text{Tx}$ were then evaluated for EMI shielding performance across the X-band frequency range of 8.2–12.4 GHz. Notably, a 15 μm film fabricated from MW- $\text{Ti}_3\text{C}_2\text{Tx}$ achieved an impressive EMI SE of approximately 67 dB, closely matching the performance of a conventional counterpart, which attained around 63 dB. The data indicates that MW-synthesized films maintain robust EMI SE across various thicknesses and frequencies. Specifically, MW- $\text{Ti}_3\text{C}_2\text{Tx}$ films with thicknesses of 5 and 10 μm demonstrated EMI SE values of 53 and 60 dB, respectively, underscoring their efficacy even at lower frequencies.

This study is the first to report the EMI SE performance of MW- $\text{Ti}_3\text{C}_2\text{Tx}$, demonstrating that MW-synthesis offers not only structural quality but also improved yield comparable to conventional methods. Our findings indicate that the EMI shielding effectiveness of MW- $\text{Ti}_3\text{C}_2\text{Tx}$ aligns well with that of conventionally synthesized MXenes in our work and also the previous literature, with the added benefits of reduced processing time, energy consumption and enhanced stability and reproducibility. This highlights a promising approach for incorporating green synthesis principles in producing high-performance MXenes, for EMI shielding applications.

2. Experimental section

2.1. Materials

Titanium aluminum carbide (Ti_3AlC_2 , ≥99 %, ≤100 μm particle size) was purchased from Nanoshel LLC. Lithium fluoride (LiF, ≥99.98 % trace metals basis) powder and Hydrochloric acid (HCl, 37 %) were purchased from Sigma Aldrich, Co., USA. Commercial MXene powder (multilayer nanoflakes, 100–200 nm thickness) was purchased from ACS Materials. The reagents were used as-received without further purification.

2.2. Synthesis of MW- $\text{Ti}_3\text{C}_2\text{Tx}$

The experimental setup for MW synthesis of $\text{Ti}_3\text{C}_2\text{Tx}$ is illustrated in detail in Fig. 1. The synthesis was carried out using an Anton Paar Monowave-400 at 2.45 GHz under sealed-vessel conditions. Initially, 0.70 g of LiF was dissolved in 15 ml of 12 M HCl, stirred for 10 min at RT, followed by the gradual addition of 1.0 g MAX powder. This mixture was then transferred to the MW reactor vessel. Utilizing temperature-controlled programming, the temperature and power were set to 110 °C and 180 W, respectively. Pulsed MW irradiation for 90 min was designed with dedicated heating and cooling profiles. Continuous stirring was maintained inside the reactor vessel (650 rpm) to avoid hot-spots. After the reaction, the mixture was washed with DI water and centrifuged at 3500 rpm until a pH of 5–6 was reached. Subsequently the slurry was dried in a vacuum oven at 120 °C for 2 h, producing MW- $\text{Ti}_3\text{C}_2\text{Tx}$ nano-powders. For comparison, $\text{Ti}_3\text{C}_2\text{Tx}$ powders (CO-MXenes) were also prepared using conventional method [28,29].

2.3. Fabrication of the MXene films

MXene films were fabricated on glass substrates using a spray coating technique. MW- $\text{Ti}_3\text{C}_2\text{Tx}$ NS were uniformly dispersed in DI water with a concentration of 15 mg/ml. By maintaining a constant flow rate, pressure, and nozzle distance from the substrate the number of spray passes were varied to achieve desired thickness (5, 10, 15 μm). Before coating, the glass slides were sonicated in isopropanol (IPA) and ethanol, followed by a 10-min plasma treatment at 50 W. After spray coating, the MXene films were dried in a vacuum oven at 80 °C for 15 min. For comparison, CO- $\text{Ti}_3\text{C}_2\text{Tx}$ films were also prepared.

2.4. Characterization

XRD data was gathered utilizing the PANalytical Empyrean system using Cu K α radiation operated in the range of 5° and 60° at 45 kV and 40 mA, employing a step size of 0.02°. The Field Emission Scanning Electron Microscopy (FESEM) images were acquired using the Quanta 600 FEG Scanning Electron Microscope. The elemental analysis for MXenes was carried out with Energy dispersive x-ray (EDX) using Quanta –600. X-ray Photoelectron Spectroscopy (XPS) was used to study the chemical composition, information about the elements present and their chemical states. XPS measurements were carried out using ThetaProbe by Thermo Fisher. Transmission Electron Microscope (TEM) images were acquired using the ThermoFisher operated at 200 kV, and a

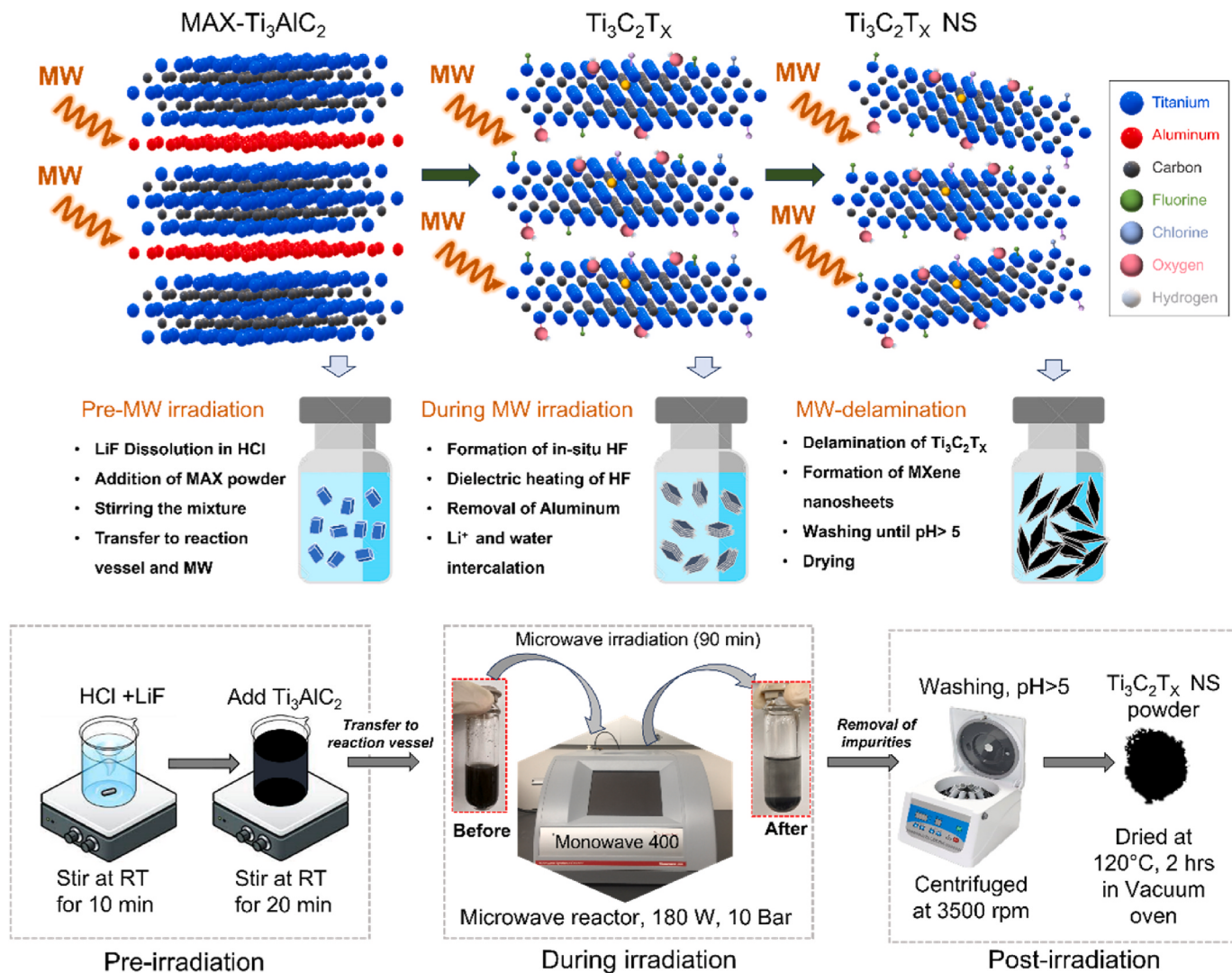


Fig. 1. Step-by-step illustration of MXene synthesis using MW-etching and delamination. The pre-MW irradiation phase involves the preparation and transfer of the solution mixture to the reaction vessel. In the MW-reactor, the reaction vessel is irradiated for 90 min. During the MW irradiation HF is produced in-situ. The Li⁺ intercalation leads to complete removal of Al and delamination of Ti₃C₂T_X sheets. This can be achieved in a short time. The precursor color was observed to change from dark grey before MW-irradiation to deep black after. MW-irradiation accelerates the removal of Al atoms from the Ti₃AlC₂ matrix facilitating efficient formation of Ti₃C₂T_X NS. The delaminated Ti₃C₂T_X are further processed by washing of MXene nano-powders and drying the supernatant solution in a vacuum oven in the post-irradiation processing stage.

lacey carbon copper grid (Ted Pella) was used for sample preparation. Raman spectroscopy was carried out with a 532 nm laser excitation source using Horiba LabRAM Soleil. X-ray total scattering measurements were conducted at the X-ray Powder Diffraction (XPD) 28-ID-2 beamline at the National Synchrotron Light Source-II (NSLS-II) at Brookhaven National Laboratory (BNL). PDF analysis was applied to the data to quantify the local atomic structure of the MXene samples. Calibration measurements were done with Ceria, and all datasets were collected at room temperature. The data acquisition, data reduction, and structural modeling for PDF analysis are described in greater detail in the supplementary information. The shielding efficacies were measured for all the samples using the two-port network analyzer (Agilent technologies 5234A) across the X-band. The samples were cut in rectangular shapes to prevent leakage from the waveguide edges. The samples were mounted and securely screwed in before the final measurements were made. A four-probe method was used to measure the electrical conductivity of the samples. To attain the conductivity of the fabricated MW-Ti₃C₂T_X films, the sheet resistance was measured using a Lucas Lab Pro4 four-point probe. The measurements were acquired at four different points on the sample films and averaged.

3. Results and discussion

Fig. 2(a) illustrates the XRD patterns depicting the transformation of Ti₃AlC₂ to exfoliated Ti₃C₂T_X sheets after varying durations of MW-irradiation. MAX phase exhibited sharp peaks at 9.6°, 19.5°, 34.1°, 38.8°, 39.6°, 41.9°, and 48.5° corresponding to (002), (004), (101), (103), (104), (105) and (107) crystal planes, respectively, as per JCPDS card 52-0875 [30]. With increased MW-duration (30–90 min), the MAX phase peaks gradually disappeared while new peaks characteristic of MXenes emerged. The (002) peak for Ti₃C₂ reached maximum intensity, indicating efficient Al removal and greater separation of MXene layers, shifting to a lower angle and signifying increased interlayer spacing [31]. Notably, the (104) peak associated with Ti₃AlC₂ vanishes entirely after 90 min, indicating high-quality Ti₃C₂T_X nanosheet (NS) formation. When the irradiation was carried out beyond the time, the (002) peak weakens and starts shifting right, suggesting disorder in MXene structure. This can be due to the overheating of MXenes and possible hotspot formation. This observation implied that, the optimal duration for MW-synthesis was 90 min [32]. For comparison, CO-Ti₃C₂T_X was also synthesized by heating the reaction mixture at 45 °C for 36 h followed by

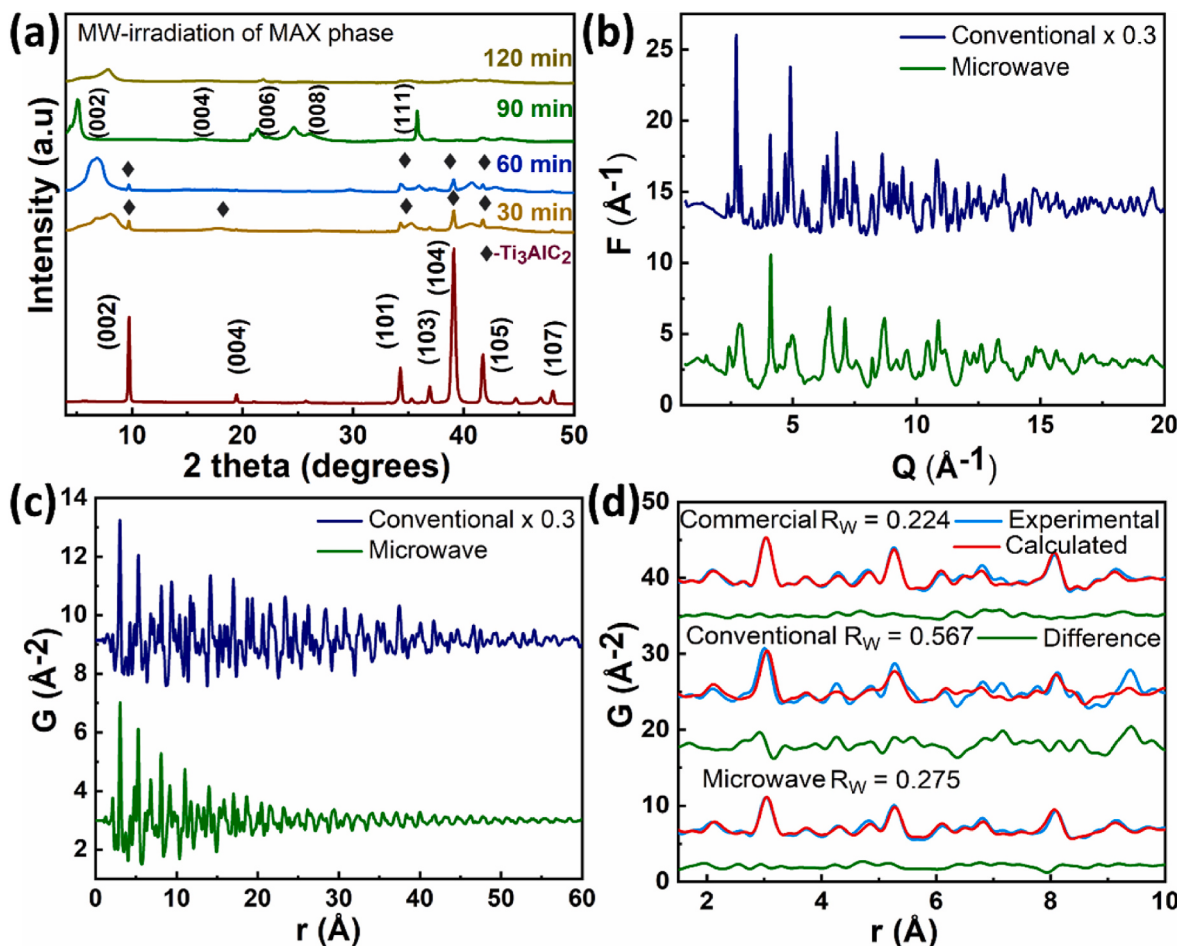


Fig. 2. (a) XRD spectra depicts the transformation of Ti_3AlC_2 MAX phase into exfoliated $\text{Ti}_3\text{C}_2\text{Tx}$ sheets at various durations of MW irradiation. The diffraction peaks related to the MAX phase disappear with increase in time of the MW irradiation, concomitant with the appearance of new peaks that are distinctive to MXenes. (b) The reduced structure function, $F(Q)$, for the $\text{Ti}_3\text{C}_2\text{Tx}$ samples synthesized via conventional methods (blue) and MW processing (green). (c) The experimental PDFs for the $\text{Ti}_3\text{C}_2\text{Tx}$ samples synthesized via conventional methods (blue) and MW processing (green). The conventional plots are scaled (by 0.3) for comparison. (d) The PDF fit results for conventionally prepared MXene sample, and MW-synthesized MXene sample from top to bottom, respectively. The experimental PDFs are in blue and the refined model PDFs are in red while the differences are offset below green. The goodness-of-fit value, or R_w , is shown in each PDF fit plot.

delamination [33]. The XRD patterns revealed persistent Al peaks even after 18 h of etching, which only disappeared with prolonged heating. This underscores the efficiency of MW-synthesis in accelerating Al removal.

The XRD of the MW-synthesized MXenes displayed broad peaks, indicating a larger lattice d-spacing compared to CO-MXenes (Fig. S1 (a)). The 20 angle corresponding to the (002) plane shifted from 8.40° ($\text{CO-Ti}_3\text{C}_2\text{Tx}$) to 6.20° (MW- $\text{Ti}_3\text{C}_2\text{Tx}$), suggesting an increase in d-spacing from $\sim 10.47 \text{ \AA}$ to $\sim 14.0 \text{ \AA}$. This increase can be attributed to the intense water and Li^+ intercalation within the MW-MXene sheets due high vapor pressure in the reactor vessel. The delamination happens in situ as Al is replaced by -OH/-F terminations [29,34]. It was observed that increasing the MW-power beyond optimal levels can damage the MXene phase-structure. At higher powers (200 and 400 W), the smooth and layered structure gives way to irregular and chipped surfaces. The acidic environment and excessive heating disrupts the crucial Ti-C bonds further compromising the integrity of the synthesized MXenes.

The PDF technique incorporates both Bragg and diffuse scattering in revealing quantitative details describing the atomic structure of nanoscale and/or disordered materials [35,36]. For materials in which structural features of interest are on the nanoscale, such as MXenes, or may deviate from long-range crystallinity, such as in MW-grown sample, where traditional crystallography alone is not sufficient to capture the atomic landscape. Therefore, total scattering PDF analysis must be

incorporated to accurately characterize local amorphous-crystalline phase mixtures. X-ray PDF analysis was used to obtain local structural information. PDF gives the scaled probability of finding two atoms at a distance ' r ' apart in a material and can be used to provide a useful, direct study of structural features within MXene [37,38]. The reduced structure function, $F(Q)$, and the experimental PDF, $G(r)$, of a conventionally prepared and MW- $\text{Ti}_3\text{C}_2\text{M}_x$ MXene sample are plotted in Fig. 2(b) and (c), respectively. In both samples, the existence of regular sharp peaks and occasional broad peaks out to high values of r as well as distinct deviations in peak shape and location between samples suggest that the structures are well ordered but also contain structural nuances, confirming the necessity for further study via PDF methods. The interatomic correlations extend further in conventional MXene samples compared to the MW samples, suggesting greater average structural coherence for the former and lower levels of long-range order in the latter. This can be seen in Fig. 2(c) where the PDF signal of the conventional MXene displays defined features out to 5 nm, in contrast to that of MW-MXene in which the structural correlations terminate around 3–4 nm. The reduction of the intensities and definition of the peaks in the high r region within the PDF from the MW sample indicates some degree of disordering in the global atomic lattice and might be associated with decrystallization or amorphization of crystalline structures, which has been attributed to MW-grown and irradiated materials in past studies for a variety of materials [39–42].

To obtain more local structural insights into the MXene samples at the sub-nanometer length scale, structural refinements were conducted in the local short-range order which represents the MXene intralayer Ti_3C_2 structure and corresponds to a PDF fit range of 1.5 Å to 10 Å. Commercial $\text{Ti}_3\text{C}_2\text{T}_x$ was measured as control sample to provide a reference benchmark for the $\text{Ti}_3\text{C}_2\text{T}_x$ structure. The hexagonal symmetry, established for well-known MAX phases (space group: $P6_3/mmc$), was used as the starting point in a structural model consisting of a single layer of Ti_3C_2 with the 3 Ti and 2C atomic layers arranged in an alternating staggered fashion [43]. The atomic displacement parameters for the Ti and C atoms were constrained to be isotropic within the layer. The result of the PDF fits is shown in Fig. 2(c). The refined structural parameters are documented in the supplementary information.

For the local fit range tested here, the MW sample demonstrated greater structural agreement with the perfectly ordered, ideal Ti_3C_2 structure when compared to the conventionally prepared counterpart. The fit results show that the peaks generally exist in the right positions, indicating that the overall local structures are correct for both conventional and MW samples. For example, the Ti-Ti bonds around 3.1 Å and 5.2 Å and the Ti-C bonds around 2.2 Å and 3.8 Å are well captured by the refined model. However, the results of the refinements to a perfect undistorted Ti_3C_2 structure also indicate the presence of unresolved structural fluctuations in the sample. This is represented by the

difference curves (offset below in green) in Fig. 2(d). In the case of the conventionally prepared MXene sample, the pronounced peaks at 7.2 Å and 9.3 Å as well as the offset peak at 3.0 Å suggest additional local correlations and variations that deviate from the Ti_3C_2 structure. These deviations might result from the structural effects of functional groups or intercalated species associated with the MXene layers in the samples.

Indeed, we expect the MXene sample structures to deviate from a pristine ordered construction for these reasons. Nevertheless, the refinements indicate that the local intralayer atomic arrangement for MW processed MXene samples resembles the ideal Ti_3C_2 phase more so than the conventionally prepared MXene samples. In conclusion, while conventional MXene sample demonstrates extended long-range order, the short-range structural fidelity to the Ti_3C_2 structure pales in comparison to that of the MW MXene sample. Possible reasons underlying the remaining misfit in the models could be the result of defects within the layers or structural distortions in the interlayer stacking, such as a turbostratic structure, which are common to 2D materials and structures [44,45]. More detailed models will be investigated in the future.

For the MXenes produced from MW-etching (Fig. 3 (a)), the SEM image shows a loosely packed, accordion-like morphology. This observation aligns well with the increased d-spacing observed in the XRD data. The micrograph also highlights clear interfaces between the exfoliated MXene sheets, suggesting greater inter-sheet separation

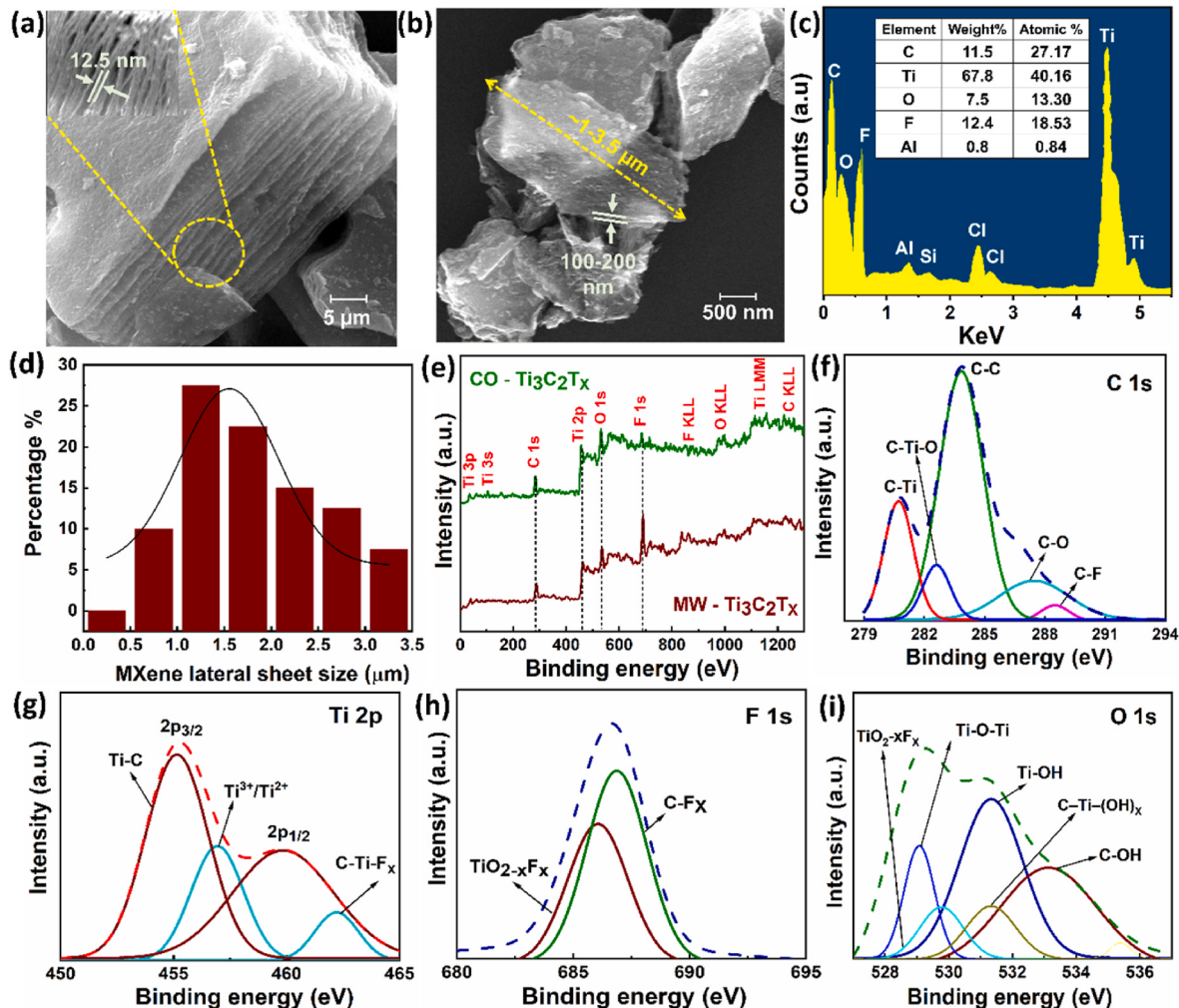


Fig. 3. (a) Morphology of MW-synthesized $\text{Ti}_3\text{C}_2\text{T}_x$ NS (Inset: magnified image of the circled area showing interlayer spacing of 12.5 nm after etching. (b) Few layered MW- $\text{Ti}_3\text{C}_2\text{T}_x$ NS after delamination. The average lateral flake size and thickness was found to be around ~1–3 µm and 100–200 nm, respectively. (c)EDX elemental spectrum and mapping. (d) Histogram summarizes the lateral sheet size distribution percentage of MW- $\text{Ti}_3\text{C}_2\text{T}_x$ NS (e) The comparison between XPS survey spectra of MW and CO- $\text{Ti}_3\text{C}_2\text{T}_x$ shows higher fluorine terminated groups in MW- $\text{Ti}_3\text{C}_2\text{T}_x$. (f) Deconvoluted C 1s core-level spectrum. (g) Deconvoluted Ti 2p spectrum highlights high quality of MXenes. (h) F 1s components of $\text{Ti}_3\text{C}_2\text{T}_x$ MXene. (i) The deconvoluted O 1s spectra.

achieved through the MW-irradiation [27]. More importantly, delamination was achieved in-situ, transforming stacked multilayered MW-Ti₃C₂T_x into few-layered NS with lateral flake-size of ~1–3.5 μm and thickness of around 100–200 nm (Fig. 3(b)). The obtained elemental spectrum as shown in Fig. 3 (c) displayed uniform and homogeneous distribution of Ti, C, F, and O. These peaks had a strong intensity while a trace amount of Al reflected as a weak peak with extremely low intensity. The elemental mapping showed that Ti₃C₂T_x contains about 11.5 wt% C, 67.8 wt% Ti, 7.5 wt% O, 12.4 wt% F, 0.8 wt% Al. The O and F can be attributed to the -OH and -F terminal groups present on the surface of MXenes. Fig. 3(d) shows the histogram summarizing the lateral sheet size distribution percentage of MW-Ti₃C₂T_x NS.

The XPS survey spectra revealed the presence of fluorine (F), carbon (C), titanium (Ti), and oxygen (O) in both samples. Notably, the F content was found to be higher in MW-Ti₃C₂T_x compared to the conventional counterpart as shown in Fig. 3(e). MW irradiation generates high temperatures and reactive environments which can enhance the incorporation of F from etching agents such as HF (formed in-situ). As a result, the rapid and localized heating may promote the formation of F-terminations over -OH groups. The absence of an Al peak in the MW-Ti₃C₂T_x spectrum confirms the effective etching of Al from the MAX phase during MW irradiation, corroborating the XRD findings and demonstrating the efficiency of the MW approach. The deconvoluted C1s core-level spectra (Fig. 3(f)) showed peaks corresponding to Ti-C (281.9 eV), C-Ti-O (283.4 eV), C-C (285 eV), C-O (287 eV), and C-F (289.4 eV) bonds [27,46]. In Fig. 3(g), the deconvoluted Ti 2p spectra revealed peaks at 455 eV and 456.5 eV, attributed to Ti-C and Ti³⁺/Ti²⁺ [47]. Furthermore, the -Fx terminated species show high stability, suggesting that fluorine terminations are less likely to introduce defects in MW-Ti₃C₂T_x compared to other terminations such as -OH and -O

groups. The high electronegativity of fluorine atoms reduces the probability of oxidation by lowering the material's chemical reactivity with atmospheric oxygen and forms a robust protective layer on the MXene surface. Consequently, the presence of F-functional group enhances the oxidation resistance of MXenes, preserving the structural integrity and electronic properties of the material [48]. The F1s XPS spectrum (Fig. 3 (h)) displayed two distinct peaks at 685.1 eV and 685.8 eV. The O 1s XPS spectrum (Fig. 3(i)) was deconvoluted into sub-peaks: Ti-O-Ti bonds at 529 eV, Ti-OH bonds at 531.8 eV, and C-OH bonds at 533.9 eV [27]. The hydroxyl groups associated with titanium (C-Ti-(OH)_x) appeared around 531.5–532.5 eV. Oxygen was found to be in a mixed oxide-fluoride environment around 530 eV (TiO₂-xF_x), indicating the partial replacement of oxygen with fluorine in the lattice [49].

Fig. 4(a) presents a TEM image of the MW-Ti₃C₂T_x NS. The inset which comprises Selected Area Electron Diffraction (SAED) pattern, acquired along the [0001] zone axis, reveals the characteristic hexagonal symmetry of MXene. This confirms the sixfold symmetry of the [0001] Ti₃C₂T_x plane and the absence of a diffused background, indicating minimal surface oxidation. This suggests a high degree of order within the lattice structure and potentially enhanced stability of the MW-Ti₃C₂T_x [50]. Fig. 4(b) shows a high-resolution TEM (HRTEM) image with a d-spacing of ~1.3 nm shown in the magnified image (Fig. 4 (c)), aligning well with the findings from the XRD data. Fast Fourier transform (FFT) has been obtained for the chosen zone using GATAN microscopy suite software as shown in Fig. 4(d). A line profile analysis was performed on the selected patterns to determine the interplanar spacing, which was measured to be 1.253 nm, as depicted in Fig. 4(e). Fig. 4(f) depicts the atomic arrangement in MW-Ti₃C₂T_x, with light and dark spots representing Ti and C atoms, respectively. The consistent multilayer arrangement of Ti and C layers, without significant

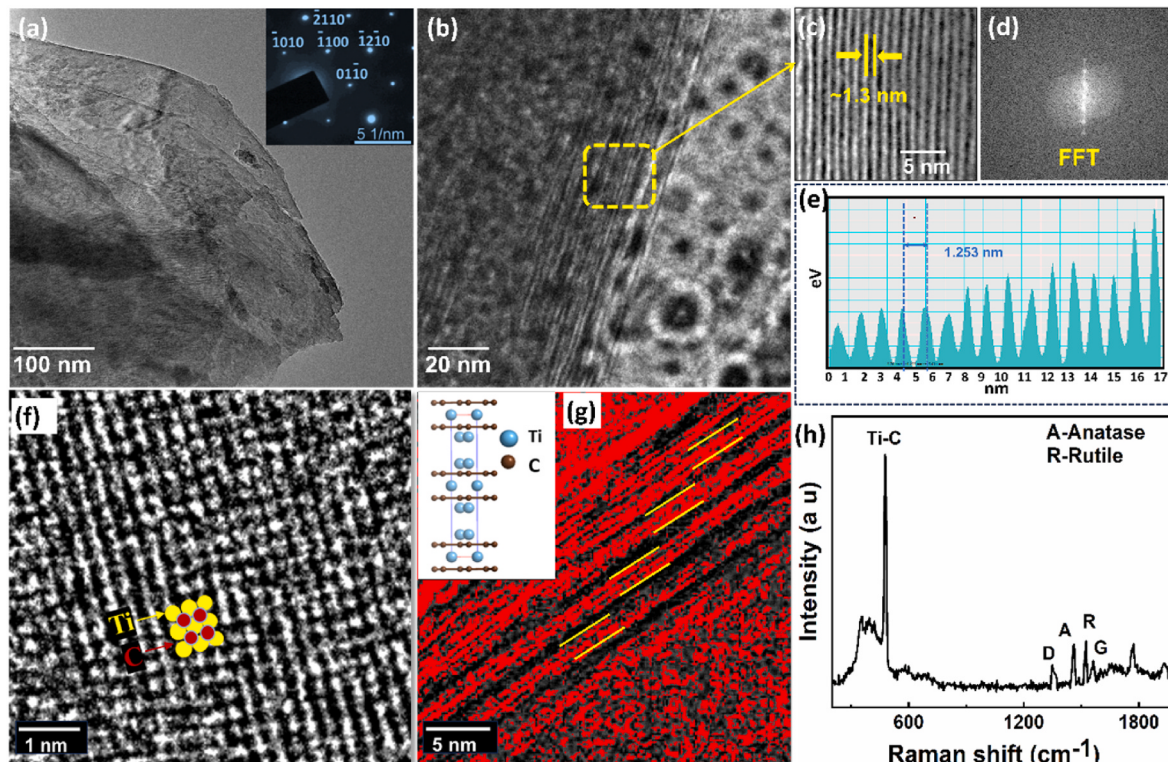


Fig. 4. (a) TEM image of MW-Ti₃C₂T_x. Inset shows the corresponding SAED pattern. (b) HRTEM image of MW-synthesized Ti₃C₂T_x nanosheets showing the d-spacing of ~1.3 nm between adjacent layers. (c) Image shows the magnified spacing. (d) Fast Fourier transform for the [0001] Ti₃C₂T_x plane. (e) Line profile indicates d-spacing. (f) The atomistic arrangement of Ti and C atoms, where the yellow circles represent Ti atoms, and the brown circles represent C atoms. (g) the multilayer arrangement of three layers of Ti and 2 layers of C between each pair of yellow lines. The TEM image has been further used for fine-tuning the threshold values until the red (layers of Ti) and black regions (layer of C) were accurately segmented which clearly show the atomic model arrangement. Inset shows the atomic structure of MXene (h)Raman spectrum of the MW-Ti₃C₂T_x shows the vibrational modes corresponding to the Ti-C, D and G graphitic carbon.

deviations from established crystallographic data, confirms that the MW-etching yields MXenes with well-defined crystal structure and minimal defects or oxidation. Fig. 4(g) illustrates the alternating arrangement of three Ti layers and two C layers observed across multiple atomic planes. Finally, in order to clearly show the atomic model arrangement, the same TEM image was used to refine thresholding parameters until the red (layers of Ti) and black (layer of C) regions were precisely segregated. The inset compares this arrangement to an atomic model generated using the ReciPro software. This model, based on the Ti_3C_2 crystallographic information file (cif) from the Materials Project database (mp-1094034, version v2023.11.1), reflects the Ti_6C_4 -type structure with six Ti atoms surrounded by two C atoms on each side.

The Raman spectrum of MW- $\text{Ti}_3\text{C}_2\text{T}_x$ NS (Fig. 4(h)) shows dominant peaks at 380 and 590 cm^{-1} , corresponding to the vibrational modes of Ti-C bonds within the MXene structure [51]. The peaks around 1450 and 1515 cm^{-1} indicate the presence of anatase and rutile phases on NS surface. The peak around 1350 and 1580 cm^{-1} are associated with the D and G bands of graphitic carbon [52]. The D-peak arises due to the presence of imperfections in the regular arrangement of carbon atoms within the graphene-like sheets of the material [53]. The G-peak originates from the in-plane vibrational mode of the sp^2 hybridized carbon atoms in the graphene sheets [53].

4. Shielding performance

The electrical conductivity and EMI shielding performance of the fabricated MW-MXene films, along with conventional reference samples (for comparison), have been thoroughly investigated. The electrical conductivity measured for MW- $\text{Ti}_3\text{C}_2\text{T}_x$ films was around $3566 \pm 5 \text{ Scm}^{-1}$, compared to $3172 \pm 12 \text{ Scm}^{-1}$ for CO- $\text{Ti}_3\text{C}_2\text{T}_x$ films. The notable decrease in electrical conductivity observed in the CO- $\text{Ti}_3\text{C}_2\text{T}_x$ films may be due to the deterioration in structural quality resulting from prolonged exfoliation times. Additionally, this contrast in conductivity can be linked to the larger lateral sheet size and enhanced oxidation resistance of the fluorine-terminated MW- $\text{Ti}_3\text{C}_2\text{T}_x$, which is produced using the microwave (MW) method in 90 min. The stability imparted by C-Ti-F_x terminations significantly have lesser proficiency to induce defects in

MXenes over time, thereby preserving their conductive properties [48]. On the other hand, the extended etching durations in conventional synthesis led to the formation of unstable titanium defect sites, which tend to aggregate into stabilized clusters. This process preferentially results in oxidation over time, producing TiO_2 and other oxide particles as Ti atoms become depleted under the harsh etching conditions [21, 48]. The defects disrupt the continuity of conductive pathways, thereby increasing electrical resistance [30]. Furthermore, the MW- technique effectively minimizes thermal gradients and localized overheating, which are potential sources of structural damage and oxidation [54]. This process results in the formation of more homogeneous films with lower junction resistance, facilitating efficient charge transport and improving the continuity of conductive pathways. Among the studied literature, MXenes with superior electrical conductivity, exhibits the highest EMI SE [48]. Thickness also plays a critical role in determining the EMI SE of a material; hence, increasing the thickness can enhance the shielding effectiveness [14]. However, practical EMI shielding applications prioritize thin films because of their lightweight and flexibility [23]. To examine this effect, we calculated theoretically the EMI SE for three films of varying thicknesses (5, 10 and 15 μm) in the X-band (8.2–12.4 GHz), as presented in Fig. 5(a). For comparison, the EMI SE of CO-MXene films with similar thicknesses was also evaluated. The plots show a quasi-linear dependence on frequency, with SE_T values gradually increasing as the frequency rises. The total EMI SE (SE_T) performance of the films has been estimated, and multiple internal reflections of the shielding layer were ignored as SE_T is greater than 15 dB.

To compare the two MXene compositions (MW and CO) with the theoretical values, we tested the EMI SE performance experimentally for MW- $\text{Ti}_3\text{C}_2\text{T}_x$ and CO- $\text{Ti}_3\text{C}_2\text{T}_x$ thin films. The experimental findings were found to be comparable to the theoretical calculations done using equation (4) in Supplementary section 6 [14]. MXene film samples (both MW and CO) achieved EMI shielding performance (SE_T) above 20 dB across the entire X-band frequency range as shown in Fig. 5 (b). This translates to over 99 % efficiency in blocking electromagnetic waves in this band [13]. The 15 μm thick MW-MXene film showed SE_T value of around 67 dB which is closely aligning to the 11.5 μm thick MXene film reported in the reference, which achieved an EMI SE of ~60 dB [14].

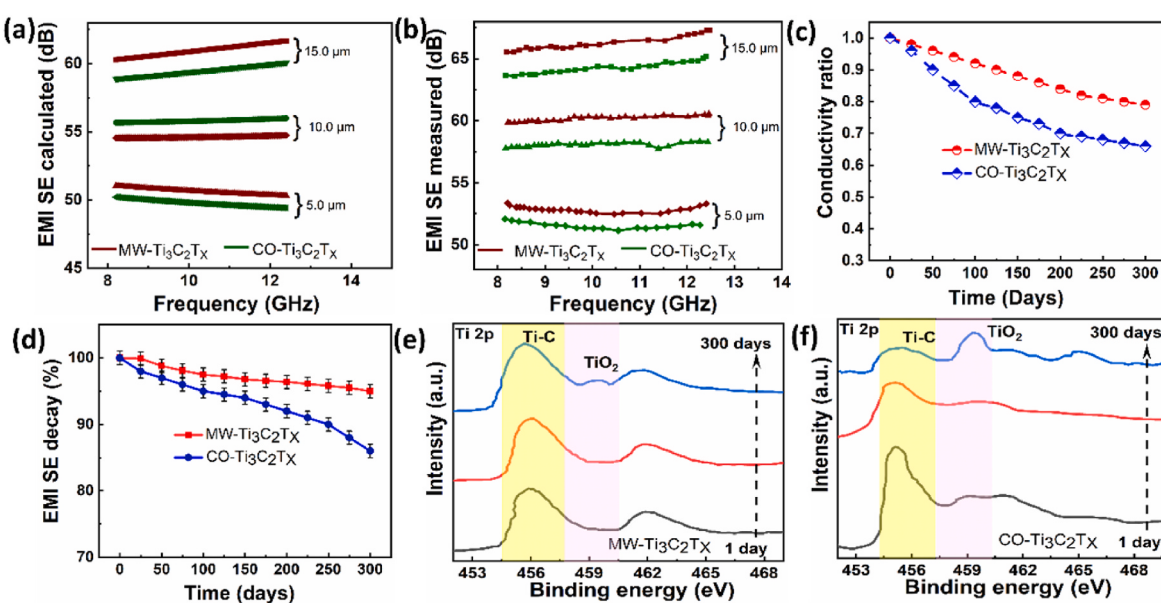


Fig. 5. (a) Theoretical EMI SE values, derived by using eq. (4)Supplementary Information (Simons formula) in X-band frequency range. (b) Experimentally measured EMI SE for MW and CO-MXene film, for 5, 10, and 15 μm spray-coated on glass substrates corroborate with the theoretical calculations. The MW-films also behave identically almost similar and show improvement than the conventionally fabricated MXene based films (c) Electrical conductivity changes measured after exposing both the MW and CO- $\text{Ti}_3\text{C}_2\text{T}_x$ devices to air over a period of 300 days. (d) EMI SE decay percentage measured over 300 days for both MW and CO-MXenes. (e) Comparison of XPS Ti 2p core spectrum of MW-MXene exposed to air for 300 days. (f) Comparison of XPS Ti 2p core spectrum of CO-MXene samples exposed to air for 300 days.

The predicted values suggest consistently comparable EMI SE for MW-based films at lower frequencies as well. Experimental data corroborates this hypothesis, demonstrating closely matching EMI SE values for MW-Ti₃C₂T_x films at 5 and 10 μm thickness exhibiting EMI SE values of 53 and 60 dB, respectively. Consequently, EMI SE performance of all the fabricated MW-MXene films not only closely match but also perform better than the CO-Ti₃C₂T_x ones. The 5, 10 and 15 μm thick CO-Ti₃C₂T_x films exhibited around 50, 56, and 63 dB, respectively.

The high structural quality of MW-Ti₃C₂T_x, achieved through shorter etching times, results in a substantial number of free electrons with high mobility. This property enables efficient nullification of incoming electromagnetic waves primarily through ohmic conduction losses, with the majority of EM waves being reflected off the MW-Ti₃C₂T_x surface. Furthermore, the absorbed EM waves are dissipated as heat during the continuous EMI shielding process.

On the other hand, CO-Ti₃C₂T_x films, which were etched for 48 h, exhibit moderate defect density. This defect density, along with functional groups, contributes to the EMI shielding mechanism through a combination of conduction losses and dipole polarization [48]. The dipole polarization occurs due to the presence of defects and functional groups in the layered structure, facilitating effective EM wave interaction [48,55]. Moreover, these moderate defects and functional groups in MW-Ti₃C₂T_x promote an impedance match, enhancing the penetration and absorption of EM waves [48]. While internal reflections contribute less at high shielding values (>15 dB), they still play a role [14]. Nonetheless, this effect can be considered within absorption, as re-reflected waves are absorbed or dissipated as heat within the material [55]. The substantial improvement in the SE_R and SE_A displayed by MW-Ti₃C₂T_x as shown in Fig. S4, supplementary material can be attributed to the higher electrical conductivity compared with CO-Ti₃C₂T_x. MW-exfoliation creates a larger MXene surface with more -F sites. These act like antennas for electromagnetic waves, leading to increased energy dissipation and improved EMI shielding. Moreover, the surfaces of MXene NS feature a combination of functional terminations, leading to a significant dielectric loss [56]. This characteristic makes them function as local dipoles when exposed to an EM field, inducing dipolar polarization [57]. Consequently, this induces added attenuation through absorption. The capability of each element to engage with incoming EM waves results in polarization losses, enhancing the effectiveness of overall shielding [58].

The total EMI shielding effectiveness (SE) values for Ti₃C₂T_x films have been compared with previously reported data, as detailed in Table S2. The MW-Ti₃C₂T_x NS films exhibit outstanding EMI shielding capabilities, demonstrating performance on par with conventional MXene synthesis methods. Remarkably, the MW-Ti₃C₂T_x films achieve an EMI SE exceeding 65 dB at a minimal thickness of 15 μm. This significant shielding efficacy is achieved in a rapid synthesis time of under 3 h. In order to explore the ambient stability, we exposed both MW and CO-MXene films to the air at the same time. As shown in Fig. 5 (c), The conductivity of the CO-MXene has gradually reduced to around 76 % of the initial conductivity after 150 days while that of MW-MXene remained at 88.2 %. At the end of 300 days the conductivity ratio of the MW-MXene remained at 80 % whereas the CO-MXene showed only 67 %. As shown in figure 5(d) it is clearly evident that the EMI SE for the CO-MXene retarded by 14 % after 300 days whereas a degradation of only 5 % was detected in the MW-MXene films suggesting superior oxidation resistance in MW-MXenes. This indicates superior oxidation resistance in MW-MXenes, which can be attributed to the fluorine terminations present in MW- Ti₃C₂T_x. The enhanced anti-oxidative stability is likely due to the rapid heating and immediate quenching applied during the MW synthesis, known as MW-thermal shocks. This process effectively removes O₂/OH terminal groups from Ti-sites within the MXene structure, thereby reducing the availability of oxidation sites. Additionally, the MW heating induces the formation and release of H₂ and vapor bubbles, increasing the vapor pressure within the reactor vessel [59]. This elevated pressure aids in the further exfoliation of

MXene sheets, enhancing the fluorine termination on the MXene surface [27]. The presence of these fluorine groups plays a crucial role in mitigating oxidation by providing a protective barrier, thus maintaining the structural integrity and performance of the MXene films over extended periods. To further validate these findings, XPS core spectrum analysis of Ti 2p was conducted for both MW-MXene and CO-MXene, as shown in Fig. 5(e)–(f), to monitor changes in termination species and composition over a 300-day period. The Ti 2p spectra of the freshly prepared MW-MXene, after just 1 day of exposure, displayed strong Ti-C peak at 455.5 eV, with no evidence of a TiO₂ peak near 459 eV. Notably, after 150 days, the Ti-C peak remained dominant in the MW-MXene, still showing no TiO₂ formation, though there was a slight reduction in Ti-C intensity. In contrast, the conventional MXene exhibited a gradual increase in TiO₂ peaks, aligning well with the conductivity measurements taken at the same time. After 300 days, the TiO₂ content in the CO-MXene further increased, corresponding with the observed 14 % decline in EMI SE performance. Meanwhile, the MW-MXene showed only gradual oxidation after 300 days, confirming that the fluorine-terminated (C-Ti-F_X) species were more stable and less prone to inducing oxidation or defects. This stability was also clearly reflected in the conductivity and EMI SE performance over time.

Further advancements in EMI shielding performance can be realized through targeted optimization of the MW-MXene synthesis processes. Tailored modifications to the surface chemistry of the MXenes can also hold promise for further enhancing their shielding capabilities. The complex interplay between microwave power, duration, temperature, and etchant conditions can make it challenging to find the "sweet spot" for desired lateral size and thickness. Therefore, by incorporating all these refinements, our future work will focus on optimizing MW-parameters to further tailor the lateral size and thickness of MXene nanosheets for EMI applications.

5. Conclusion

In summary, our work demonstrates an efficient approach for synthesizing Ti₃C₂T_x-MXenes using MW-selective etching of its MAX phase. This method significantly expedites processing while enhancing inter-sheet spacing and improving the local atomic ordering within the MXene structure. XRD and PDF studies reveal that MW-synthesized Ti₃C₂T_x possesses a short-range atomic arrangement closer to the ideal Ti₃C₂ structure compared to conventionally produced samples. This superior structural fidelity translates to exceptional EMI SE performance, particularly evident in few layered MW- Ti₃C₂T_x NS obtained via MW-exfoliation. Furthermore, the introduction of additional surface termination groups (-F, -OH/=O) during intercalation process creates centres for dipole polarization losses, significantly enhancing EM wave absorption. The XPS analysis also shows that fluorine terminations, in particular, play a critical role in improving anti-oxidative stability. Notably, this innovative method also delivers a remarkable ~75 % reduction in energy consumption and production costs compared to traditional etching and delamination techniques.

The MW method facilitates faster synthesis times and eliminates the need for additional exfoliation or delamination techniques required in conventional methods, which are time-consuming and less efficient. MW-synthesized MXenes exhibit comparable, and in-fact better performance in terms of structural integrity and EMI SE. Our findings highlight the significant advantages of MW-assisted synthesis for producing high-quality MXenes. Remarkably, the MW- Ti₃C₂T_x films achieve an EMI SE of ~67 dB at a minimal thickness of 15 μm. Additionally, thinner films with thicknesses of 5 and 10 μm exhibit EMI SE values of 53 dB and 60 dB, respectively, demonstrating effective shielding over a broad frequency spectrum.

Moving forward, we will further optimize MW parameters to achieve control over the lateral size and thickness of MXene nanosheets, aiming for optimal EMI shielding performance. Ultimately, integrating these MW-synthesized MXenes into functional devices and assessing their

real-world EMI shielding effectiveness, which consistently demonstrates SE values of over 60 dB, will be essential for their practical implementation.

CRediT authorship contribution statement

H. Renuka: Writing – review & editing, Writing – original draft, Visualization, Supervision, Methodology, Investigation, Formal analysis, Data curation, Conceptualization. **Morgan Chen:** Writing – original draft, Investigation, Formal analysis. **Shwetha Sunil Kumar:** Writing – review & editing, Investigation, Formal analysis. **Long Yang:** Writing – review & editing, Investigation, Formal analysis, Conceptualization. **Michael T. Lanagan:** Writing – review & editing, Supervision, Conceptualization. **Sanjit Ghose:** Writing – review & editing, Validation, Supervision, Methodology, Data curation. **B. Rejea-Jayan:** Writing – review & editing, Supervision, Funding acquisition.

Declaration of competing interest

The authors have no interests to declare.

Data availability

Data will be made available on request.

Acknowledgements

This material is based upon work supported by the Air Force Office of Scientific Research under award number FA9550-22-1-0308. This work is also supported by the National Science Foundation Graduate Research Fellowship Program under Grant No. DGE2140739. Any opinions, findings, and conclusions or recommendations expressed in this material are those of the author(s) and do not necessarily reflect the views of the United States Air Force or the National Science Foundation. The authors would also like to acknowledge the use of the Materials Characterization Facility at Carnegie Mellon University supported by grant MCF-677785.

Appendix A. Supplementary data

Supplementary data to this article can be found online at <https://doi.org/10.1016/j.mssp.2024.108966>.

References

- [1] G. Dastgeer, et al., Atomically engineered, high-speed non-volatile flash memory device exhibiting multibit data storage operations, *Nano Energy* 119 (2024), <https://doi.org/10.1016/j.nanoen.2023.109106>.
- [2] G. Dastgeer, A.M. Afzal, G. Nazir, N. Sarwar, p-GeSe/n-ReS₂ heterojunction rectifier exhibiting A fast photoresponse with ultra-high frequency-switching applications, *Adv. Mater. Interfac.* 8 (22) (2021), <https://doi.org/10.1002/admi.202100705>.
- [3] L.M. Zhang, et al., Structural and optical study of irradiation effect in GaN epilayers induced by 308 MeV Xe ions, *Nucl. Instrum. Methods Phys. Res. B* 269 (15) (2011), <https://doi.org/10.1016/j.nimb.2011.04.118>.
- [4] M. Khazaei, A. Mishra, N.S. Venkataraman, A.K. Singh, S. Yunoki, Recent Advances in MXenes: from Fundamentals to Applications, 2019, <https://doi.org/10.1016/j.cossms.2019.01.002>.
- [5] S. Fatima, I.H. Sajid, M.F. Khan, S. Rizwan, Synthesis and characterization of erbium decorated V2CTx for water splitting properties, *Int. J. Hydrogen Energy* 55 (2024), <https://doi.org/10.1016/j.ijhydene.2023.11.114>.
- [6] R. Tahir, M.W. Hakim, A. Murtaza, M.F. Khan, S. Rizwan, First observation of induced ferroelectric and magnetoelectric properties in pristine and Ni-intercalated Mo₂TiC2Tx double transition metal MXene, *Adv Electron Mater* 9 (12) (2023), <https://doi.org/10.1002/aelm.202300299>.
- [7] Y. Wang, Y. Wang, Recent Progress in MXene Layers Materials for Supercapacitors: High-Performance Electrodes, 2023, <https://doi.org/10.1002/smm2.1130>.
- [8] M. Naguib, M.W. Barsoum, Y. Gogotsi, Ten years of progress in the synthesis and development of MXenes, *Adv. Mater.* 33 (39) (2021), <https://doi.org/10.1002/adma.202103393>.
- [9] M. Naguib, V.N. Mochalin, M.W. Barsoum, Y. Gogotsi, 25th anniversary article: MXenes: a new family of two-dimensional materials, *Adv. Mater.* 26 (7) (2014), <https://doi.org/10.1002/adma.201304138>.
- [10] S. Wan, et al., High-strength scalable MXene films through bridging-induced densification, *Science* 374 (6563) (2021), <https://doi.org/10.1126/science.abbg2026>, 1979.
- [11] T. Yun, et al., Electromagnetic interference shielding: electromagnetic shielding of monolayer MXene assemblies (*adv. Mater.* 9/2020), *Adv. Mater.* 32 (9) (2020), <https://doi.org/10.1002/adma.202070064>.
- [12] M.H. Al-Saleh, U. Sundararaj, Electromagnetic interference shielding mechanisms of CNT/polymer composites, *Carbon N Y* 47 (7) (2009), <https://doi.org/10.1016/j.carbon.2009.02.030>.
- [13] M. Han, et al., Beyond Ti3C2Tx: MXenes for electromagnetic interference shielding, *ACS Nano* 14 (4) (2020), <https://doi.org/10.1021/acsnano.0c01312>.
- [14] F. Shahzad, et al., Electromagnetic interference shielding with 2D transition metal carbides (MXenes), *Science* 353 (6304) (2016), <https://doi.org/10.1126/science.aag2421>, 1979.
- [15] J. Zhang, et al., Scalable manufacturing of free-standing, strong Ti3C2Tx MXene films with outstanding conductivity, *Adv. Mater.* 32 (23) (2020), <https://doi.org/10.1002/adma.202001093>.
- [16] X. Wu, et al., Direct ink writing of highly conductive MXene frames for tunable electromagnetic interference shielding and electromagnetic wave-induced thermochromism, *Nano-Micro Lett.* 13 (1) (2021), <https://doi.org/10.1007/s40820-021-00665-9>.
- [17] A. Feng, et al., Two-dimensional MXene Ti3C2 produced by exfoliation of Ti3AlC₂, *Mater. Des.* 114 (2017), <https://doi.org/10.1016/j.matdes.2016.10.053>.
- [18] Y. Ying, et al., Two-dimensional titanium carbide for efficiently reductive removal of highly toxic chromium(VI) from water, *ACS Appl. Mater. Interfaces* 7 (3) (2015), <https://doi.org/10.1021/am5074722>.
- [19] O. Mashatalir, M.R. Lukatskaya, M.Q. Zhao, M.W. Barsoum, Y. Gogotsi, Amine-assisted delamination of Nb2C MXene for li-ion energy storage devices, *Adv. Mater.* 27 (23) (2015), <https://doi.org/10.1002/adma.201500604>.
- [20] M. Alhabeb, et al., Guidelines for synthesis and processing of two-dimensional titanium carbide (Ti3C2Tx MXene), *Chem. Mater.* 29 (18) (2017), <https://doi.org/10.1021/acs.chemmater.7b02847>.
- [21] A. Iqbal, J. Hong, T.Y. Ko, C.M. Koo, Improving Oxidation Stability of 2D MXenes: Synthesis, Storage Media, and Conditions, 2021, <https://doi.org/10.1186/s40580-021-00259-6>.
- [22] M. Dadashi Firouzjaei, S.K. Nemaní, M. Sadrzadeh, E.K. Wujcik, M. Elliott, B. Anasori, Life-cycle assessment of Ti3C2Tx MXene synthesis, *Adv. Mater.* 35 (31) (2023), <https://doi.org/10.1002/adma.202300422>.
- [23] F.M. Oliveira, J. Azadmanjiri, X. Wang, M. Yu, Z. Sofer, Structure Design and Processing Strategies of MXene-Based Materials for Electromagnetic Interference Shielding, 2023, <https://doi.org/10.1002/smtd.202300112>.
- [24] A.A. Oladipo, Microwave-assisted synthesis of high-performance polymer-based nanoadsorbents for pollution control, in: New Polymer Nanocomposites for Environmental Remediation, 2018, <https://doi.org/10.1016/B978-0-12-811033-1.00014-7>.
- [25] W. Cai, et al., Microwave-assisted reduction and sintering to construct hybrid networks of reduced graphene oxide and MXene for electromagnetic interference shielding, *Composer Part A Appl Sci Manuf* 157 (2022), <https://doi.org/10.1016/j.compositesa.2022.106928>.
- [26] J. Zhu, et al., Rapid one-step scalable microwave synthesis of Ti3C2T: XMXene, *Chem. Commun.* 57 (94) (2021), <https://doi.org/10.1039/c1cc04989e>.
- [27] A. Numan, et al., Microwave-assisted rapid MAX phase etching and delamination: a paradigm shift in MXene synthesis, *Mater. Chem. Phys.* 288 (2022), <https://doi.org/10.1016/j.matchemphys.2022.126429>.
- [28] M.D. Wagh, H. Renuka, P.S. Kumar, K. Amreen, S.K. Sahoo, S. Goel, Integrated microfluidic device with MXene enhanced laser-induced graphene bioelectrode for sensitive and selective electroanalytical detection of dopamine, *IEEE Sensor. J.* 22 (14) (2022), <https://doi.org/10.1109/JSEN.2022.3182293>.
- [29] O. Mashatalir, M. Naguib, B. Dyatkin, Y. Gogotsi, M.W. Barsoum, Kinetics of aluminum extraction from Ti3AlC₂ in hydrofluoric acid, *Mater. Chem. Phys.* 139 (1) (2013), <https://doi.org/10.1016/j.matchemphys.2013.01.008>.
- [30] Z. Li, et al., Synthesis and thermal stability of two-dimensional carbide MXene Ti3C2, *Mater. Sci. Eng., B* 191 (C) (2015), <https://doi.org/10.1016/j.mseb.2014.10.009>.
- [31] L. Verger, V. Natu, M. Carey, M.W. Barsoum, MXenes: an Introduction of Their Synthesis, Select Properties, and Applications, 2019, <https://doi.org/10.1016/j.trechn.2019.04.006>.
- [32] W. Sun, et al., Electrochemical etching of Ti2AlC to Ti2CT:X (MXene) in low-concentration hydrochloric acid solution, *J Mater Chem A Mater* 5 (41) (2017), <https://doi.org/10.1039/c7ta05574a>.
- [33] M. Naguib, et al., Two-dimensional nanocrystals: two-dimensional nanocrystals produced by exfoliation of Ti3AlC₂ (adv. Mater. 37/2011), *Adv. Mater.* 23 (37) (2011), <https://doi.org/10.1002/adma.201190147>.
- [34] H.W. Wang, M. Naguib, K. Page, D.J. Wesolowski, Y. Gogotsi, Resolving the structure of Ti3C2Tx MXenes through multilevel structural modeling of the atomic pair distribution function, *Chem. Mater.* 28 (1) (2016), <https://doi.org/10.1021/acs.chemmater.5b04250>.
- [35] T.L. Christiansen, S.R. Cooper, K.M.O. Jensen, There's no place like real-space: elucidating size-dependent atomic structure of nanomaterials using pair distribution function analysis, *Nanoscale Adv.* 2 (6) (2020), <https://doi.org/10.1039/d0na00120a>.
- [36] M.W. Terban, S.J.L. Billinge, Structural Analysis of Molecular Materials Using the Pair Distribution Function, 2022, <https://doi.org/10.1021/acs.chemrev.1c00237>.
- [37] S.J.L. Billinge, Nanometre-scale Structure from Powder Diffraction: Total Scattering and Atomic Pair Distribution Function Analysis, 2019, <https://doi.org/10.1107/97809553602060000972>.

- [38] M. Shekhirev, C.E. Shuck, A. Sarycheva, Y. Gogotsi, Characterization of MXenes at Every Step, from Their Precursors to Single Flakes and Assembled Films, 2021, <https://doi.org/10.1016/j.jpmatsci.2020.100757>.
- [39] R. Roy, Y. Fang, J. Cheng, D.K. Agrawal, Decrystallizing solid crystalline titania, without melting, using microwave magnetic fields, *J. Am. Ceram. Soc.* 88 (6) (2005), <https://doi.org/10.1111/j.1551-2916.2005.00261.x>.
- [40] A. Nozariasmarz, K. Dsouza, D. Vashaee, Field induced decrystallization of silicon: evidence of a microwave non-thermal effect, *Appl. Phys. Lett.* 112 (9) (2018), <https://doi.org/10.1063/1.5020192>.
- [41] N. Nakamura, et al., Linking far-from-equilibrium defect structures in ceramics to electromagnetic driving forces, *J Mater Chem A Mater* 9 (13) (2021), <https://doi.org/10.1039/dta00486g>.
- [42] N. Nakamura, M.W. Terban, S.J.L. Billinge, B. Reeja-Jayan, Unlocking the structure of mixed amorphous-crystalline ceramic oxide films synthesized under low temperature electromagnetic excitation, *J Mater Chem A Mater* 5 (35) (2017), <https://doi.org/10.1039/c7ta06339c>.
- [43] M. Ghidiu, et al., "ChemInform abstract: synthesis and characterization of two-dimensional Nb 4 C 3 (MXene).", *ChemInform* 45 (40) (2014) <https://doi.org/10.1002/chin.201440016>.
- [44] B. Anasori, et al., Control of electronic properties of 2D carbides (MXenes) by manipulating their transition metal layers, *Nanoscale Horiz* 1 (3) (2016), <https://doi.org/10.1039/c5nh00125k>.
- [45] C. Shi, M. Beidaghi, M. Naguib, O. Mashtalir, Y. Gogotsi, S.J.L. Billinge, Structure of nanocrystalline Ti3 C2 MXene using atomic pair distribution function, *Phys. Rev. Lett.* 112 (12) (2013), <https://doi.org/10.1103/PhysRevLett.112.125501>.
- [46] G.B. Soares, B. Bravin, C.M.P. Vaz, C. Ribeiro, Facile synthesis of N-doped TiO₂ nanoparticles by a modified polymeric precursor method and its photocatalytic properties, *Appl. Catal., B* 106 (3–4) (2011), <https://doi.org/10.1016/j.apcatb.2011.05.018>.
- [47] J. Zhu, Y. Tang, C. Yang, F. Wang, M. Cao, " composites of TiO₂ nanoparticles deposited on Ti 3 C 2 MXene nanosheets with enhanced electrochemical performance ,", *J. Electrochem. Soc.* 163 (5) (2016) <https://doi.org/10.1149/2.0981605jes>.
- [48] K. Rajavel, X. Yu, P. Zhu, Y. Hu, R. Sun, C. Wong, Exfoliation and defect control of two-dimensional few-layer MXene Ti3C2T xfor electromagnetic interference shielding coatings, *ACS Appl. Mater. Interfaces* 12 (44) (2020), <https://doi.org/10.1021/acsami.0c12835>.
- [49] E.V. Astrova, et al., Titanium oxyfluoride as a material for negative electrodes of lithium-ion batteries, *Int. J. Mol. Sci.* 24 (5) (2023), <https://doi.org/10.3390/ijms24054968>.
- [50] H. Ahmed, et al., Recovery of oxidized two-dimensional MXenes through high frequency nanoscale electromechanical vibration, *Nat. Commun.* 14 (1) (2023), <https://doi.org/10.1038/s41467-022-34699-3>.
- [51] T. Ohsaka, F. Izumi, Y. Fujiki, Raman spectrum of anatase, TiO₂, *J. Raman Spectrosc.* 7 (6) (1978), <https://doi.org/10.1002/jrs.1250070606>.
- [52] A.C. Khot, T.D. Dongale, J.H. Park, A.V. Kesavan, T.G. Kim, Ti3C2-Based MXene oxide nanosheets for resistive memory and synaptic learning applications, *ACS Appl. Mater. Interfaces* 13 (4) (2021), <https://doi.org/10.1021/acsami.0c19028>.
- [53] J. Bin Wu, M.L. Lin, X. Cong, H.N. Liu, P.H. Tan, Raman Spectroscopy of Graphene-Based Materials and its Applications in Related Devices, 2018, <https://doi.org/10.1039/c6cs00915h>.
- [54] I. Bilecka, M. Niederberger, Microwave chemistry for inorganic nanomaterials synthesis, *Nanoscale* 2 (8) (2010), <https://doi.org/10.1039/b9nr00377k>.
- [55] M.H. Al-Saleh, W.H. Saadeh, U. Sundararaj, EMI shielding effectiveness of carbon based nanostructured polymeric materials: a comparative study, *Carbon N Y* 60 (2013), <https://doi.org/10.1016/j.carbon.2013.04.008>.
- [56] K. Raagulan, et al., An effective utilization of MXene and its effect on electromagnetic interference shielding: flexible, free-standing and thermally conductive composite from MXene-PAT-poly(P-aminophenol)-polyaniline co-polymer, *RSC Adv.* 10 (3) (2020), <https://doi.org/10.1039/c9ra09522e>.
- [57] M. Peng, F. Qin, Clarification of basic concepts for electromagnetic interference shielding effectiveness, *J. Appl. Phys.* 130 (22) (2021), <https://doi.org/10.1063/5.0075019>.
- [58] A. Iqbal, et al., Anomalous absorption of electromagnetic waves by 2D transition metal carbonitride Ti3CNTx(MXene), *Science* 369 (6502) (2020), <https://doi.org/10.1126/science.aba7977>, 1979.
- [59] Y.J. Zhu, F. Chen, Microwave-assisted Preparation of Inorganic Nanostructures in Liquid Phase, 2014, <https://doi.org/10.1021/cr400366s>.